Acta Biomaterialia 70 (2018) 177–185

Contents lists available at ScienceDirect

Acta Biomaterialia

journal homepage: www.elsevier.com/locate/actabiomat

Full length article

Lung cancer specific and reduction-responsive chimaeric polymersomes for highly efficient loading of pemetrexed and targeted suppression of lung tumor *in vivo*

Weijing Yang [a], Liang Yang [a], Yifeng Xia [a], Liang Cheng [a,b,*], Jian Zhang [a], Fenghua Meng [a,*], Jiandong Yuan [c], Zhiyuan Zhong [a,*]

[a] Biomedical Polymers Laboratory, and Jiangsu Key Laboratory of Advanced Functional Polymer Design and Application, College of Chemistry, Chemical Engineering and Materials Science, Soochow University, Suzhou 215123, PR China
[b] Department of Pharmaceutics, College of Pharmaceutical Sciences, Soochow University, Suzhou 215123, PR China
[c] BrightGene Bio-Medical Technology Co., Ltd., Suzhou 215123, PR China

ARTICLE INFO

Article history:
Received 11 November 2017
Received in revised form 11 January 2018
Accepted 12 January 2018
Available online 14 February 2018

Keywords:
Polymersomes
Reduction-sensitive
Targeted delivery
Pemetrexed
Lung cancer

ABSTRACT

Lung cancer is one of the worldwide leading and fast-growing malignancies. Pemetrexed disodium (PEM, Alimta®), a small hydrophilic drug, is currently used for treating lung cancer patients. However, PEM suffers from issues like fast elimination, low bioavailability, poor tumor cell selectivity and penetration. Here, we report on lung cancer specific CSNIDARAC (CC_9) peptide-functionalized reduction-responsive chimaeric polymersomes (CC_9-RCPs) for efficient encapsulation and targeted delivery of PEM to H460 human lung cancer cells *in vitro* and *in vivo*. PEM-loaded CC_9-RCPs (PEM-CC_9-RCPs) was obtained from co-self-assembly of poly(ethylene glycol)-*b*-poly(trimethylene carbonate-*co*-dithiolane trimethylene carbonate)-*b*-polyethylenimine (PEG-P(TMC-DTC)-PEI) and CC_9-functionalized PEG-P(TMC-DTC) in the presence of PEM followed by self-crosslinking. PEM-CC_9-RCPs displayed an optimal CC_9 density of 9.0% in targeting H460 cells, a high PEM loading content of 14.2 wt%, a small hydrodynamic size of ca. 60 nm and glutathione-triggered PEM release. MTT assays showed that PEM-CC_9-RCPs was 2.6- and 10- fold more potent to H460 cells than the non-targeting PEM-RCPs and free PEM controls, respectively. Interestingly, PEM-CC_9-RCPs exhibited 22-fold longer circulation time and 9.1-fold higher accumulation in H460 tumor than clinical formulation Alimta®. Moreover, CC_9-RCPs showed obviously better tumor penetration than RCPs. Remarkably, PEM-CC_9-RCPs at 12.5 mg PEM equiv./kg effectively suppressed growth of H460 xenografts and significantly prolonged mouse survival time as compared to PEM-RCPs and Alimta® controls. These lung cancer specific and reduction-responsive chimaeric polymersomes provide a unique pemetrexed nanoformulation for targeted lung cancer therapy.

Statement of Significance

Multitargeted antifolate agent pemetrexed (PEM, Alimta®) is currently used for treating lung cancer patients and has low side-effects. However, PEM suffers from issues like fast elimination, low bioavailability, poor tumor cell selectivity and penetration. Scarce work on targeted delivery of PEM has been reported, partly because most conventional nanocarriers show a low and instable loading for hydrophilic, negatively charged drugs like PEM. Herewith, we report on lung cancer specific CSNIDARAC (CC_9) peptide-functionalized reduction-responsive chimaeric polymersomes (CC_9-RCPs) which showed efficient PEM encapsulation (14.2 wt%, 60 nm) and targeted delivery of PEM to H460 human lung cancer cells, leading to effective suppression of H460 tumor xenografts and significantly prolonged survival rates of mice than Alimta®. To the best of our knowledge, this represents a first report on targeted nanosystems that are capable of efficient loading and targeted delivery of PEM to lung tumors.

* Corresponding authors at: Biomedical Polymers Laboratory, and Jiangsu Key Laboratory of Advanced Functional Polymer Design and Application, College of Chemistry, Chemical Engineering and Materials Science, Soochow University, Suzhou 215123, PR China.
E-mail addresses: chengliang1983@suda.edu.cn (L. Cheng), fhmeng@suda.edu.cn (F. Meng), zyzhong@suda.edu.cn (Z. Zhong).

https://doi.org/10.1016/j.actbio.2018.01.015
1742-7061/

Introduction

Lung cancer, among which over 80% is non-small cell lung cancer (NSCLC), becomes one of the worldwide leading and fast growing malignancies [1]. Targeted chemotherapy using Iressa, Tarceva and Camry, though could prolong the survival 2–3 times for patients with EGFR-mutant lung cancer, is not effective to majority of NSCLC patients that are EGFR mutation-negative [2,3]. Chemotherapeutics including *cis*-platinum, carboplatin, paclitaxel (PTX), docetaxel (DTX) and pemetrexed disodium (PEM) are routinely used for treating NSCLC in the clinical settings [4–6]. Notably, PEM, a folate antimetabolite inhibiting DNA and RNA synthesis in cancer cells [4], has received particular attention because it is a multitargeted antifolate agent and has relatively less side-effects [7–9]. PEM for injection (Alimta®) is a second-line drug for NSCLC and first-line drug for malignant pleural mesothelioma [10,11]. However, clinical use of PEM suffers from several problems like fast elimination, low bioavailability, poor tumor cell selectivity and penetration, and potential spleen and kidney toxicity [12,13].

It is interesting to note that despite its clinical significance, scarce work on targeted delivery of PEM has been reported. This is partly due to the fact that most conventional nanocarriers including liposomes, nanoparticles, and micelles show a low and instable loading for hydrophilic, negatively charged, and small drugs like methotrexate disodium (MTX) and PEM [14–16]. For example, a low PEM loading efficiency of <14% was reported for liposomes [17]. We recently reported that chimaeric polymersomes with short polycations such as PDMA and PEI in the watery interior achieved highly efficient and stable encapsulation of MTX and siRNA [18,19].

Here, we report for the first time on lung cancer specific CSNIDARAC peptide-functionalized and reduction-responsive chimaeric polymersomes (CC_9-RCPs) for efficient encapsulation and targeted delivery of PEM to H460 human lung cancer cells *in vitro* and *in vivo* (Scheme 1). PEM-CC_9-RCPs were readily prepared by co-self-assembly of poly(ethylene glycol)-*b*-poly(trimethylene carbonate-*co*-dithiolane trimethylene carbonate)-*b*-polyethylenimine (PEG-P(TMC-DTC)-PEI) and CC_9-functionalized PEG-P(TMC-DTC) copolymers in the presence of PEM. CC_9 peptide screened by phage display technology was shown to be specific to lung cancer cells such as H460 cells [20]. CC_9-RCPs were expected to be self-crosslinkable, robust, and glutathione-responsive, as previously reported for dithiolane trimethylene carbonate (DTC)-containing polymersomes and micelles [21,22]. Strikingly, PEM-loaded CC_9-RCPs show significantly enhanced *in vitro* antitumor activity, circulation time, as well as tumor accumulation and suppression in human H460 lung tumor-bearing nude mice as compared to the clinical formulation Alimta®. These lung cancer specific and reduction-responsive chimaeric polymersomes provide a unique pemetrexed nanoformulation for targeted lung cancer therapy.

Experimental

2.1. Preparation of CC_9-RCPs and PEM-CC_9-RCPs

PEM-CC_9-RCPs and CC_9-RCPs were prepared from co-self-assembly of PEG-P(TMC-DTC)-PEI [19] and CC_9-PEG-P(TMC-DTC) at CC_9 molar ratios of 0, 4.5%, 9.0% or 13.5%. Briefly, 50 μL of mixed polymer solution in DMSO (10 mg/mL) was injected into 0.95 mL of HEPES buffer (pH 5.5, 5 mM) with or without PEM. After standing still for 20 min, the polymersomes were gently mixed and placed into shaking bath (200 rpm, 37 °C) for 12 h and followed by extensive dialysis for 24 h (MWCO 3500). Dynamic light scattering (DLS), static light scattering (SLS) and TEM measurements were measured. The drug loading content (DLC) and drug loading efficiency (DLE) of PEM were determined with UV–Vis spectroscopy at 246 nm. The *in vitro* PEM release was studied at polymersome concentration of 100 μg/mL using HPLC as described in supporting information.

2.2. MTT assays

H460 cells were seeded in a 96-well plate (5×10^3 cells/well) and cultured for 24 h using RPMI-1640 medium supplemented with 10% fetal bovine serum (FBS), 1% L-glutamine (final conc. 2 mM), antibiotics penicillin (100 IU/mL) and streptomycin (100 μg/mL). For assessment of their targeting effect, PEM-CC_9-RCPs with CC_9 molar ratio of 0, 4.5%, 9.0% or 13.5% (PEM concentration: 5 μg/mL) were added. The cells were incubated in an atmosphere containing 5% CO_2 at 37 °C for 4 h. The culture medium was replaced with fresh medium and the cells were incubated for 68 h. MTT assays (3-(4,5-dimethylthiazol-2-yl)-2,5-diphenyltetrazoliumbromide) were performed as described in our previous report [23]. PEM-RCPs and free PEM were used as controls.

For determination of the half-maximal inhibitory concentration (IC_{50}), H460 cells were incubated with PEM-CC_9-RCPs with 9.0 mol.% CC_9, PEM-RCPs or free PEM in 20 μL PB (PEM concentrations: 0.001–20 μg/mL) for 4 h. The rest was performed as above. The IC_{50} values were derived by fitting the cell viability data using Prism 7. For evaluation of the cytotoxicity of empty polymersomes, H460 cells were incubated with CC_9-RCPs and RCPs at varying concentrations of 0.1, 0.3 and 0.5 mg/mL at 37 °C for 48 h before MTT assays.

2.3. Animal models

All animal experiments were approved by the Animal Care and Use Committee of Soochow University (P.R. China) and all protocols of animal studies conformed to the Guide for the Care and Use of Laboratory Animals. For analysis of blood circulation, female Balb/c mice (18–22 g) were used. Mice bearing H460 tumor xenografts were built by subcutaneous injection of 0.05 mL of H460 cells (1×10^7) into the right hind flank of female nude mice. Tumor inhibition experiments started when the tumors reached 100 mm^3 after ca. 2 weeks. At tumor size of 150–200 mm^3, tumor penetration of polymersomes was studied. At tumor size of 200–300 mm^3, the *in vivo* imaging and biodistribution experiments were conducted. Before each experiment, the mice were weighed and randomly grouped.

2.4. *Biodistribution of PEM-CC_9-RCPs in H460 tumor bearing nude mice*

A single dose of PEM-CC_9-RCPs or PEM-RCPs in 0.2 mL PB was administrated into H460 tumor bearing mice via tail veins at 12.5 mg PEM equiv./kg. At 8 h post injection, the mice were sacrificed, the tumors and major organs were collected, and homogenized and treated as described in previous report [18] before PEM determination by HPLC (expressed as percentage of injected dose per gram of tissue, %ID/g).

2.5. *Tumor penetration of PEM/Cy5-CC_9-RCPs*

To investigate PEM accumulation and penetration in the tumors, PEM and Cy5-sulfo co-loaded polymersomes, i.e. PEM/Cy5-CC_9-RCPs and PEM/Cy5-RCPs were prepared and used to track the location of drugs in the tumors. A single dose of PEM/Cy5-CC_9-RCPs or PEM/Cy5-RCPs in 0.2 mL of PB (0.4 μmol Cy5 equiv./kg, 12.5 mg PEM equiv./kg) was injected via tail veins into H460 tumor

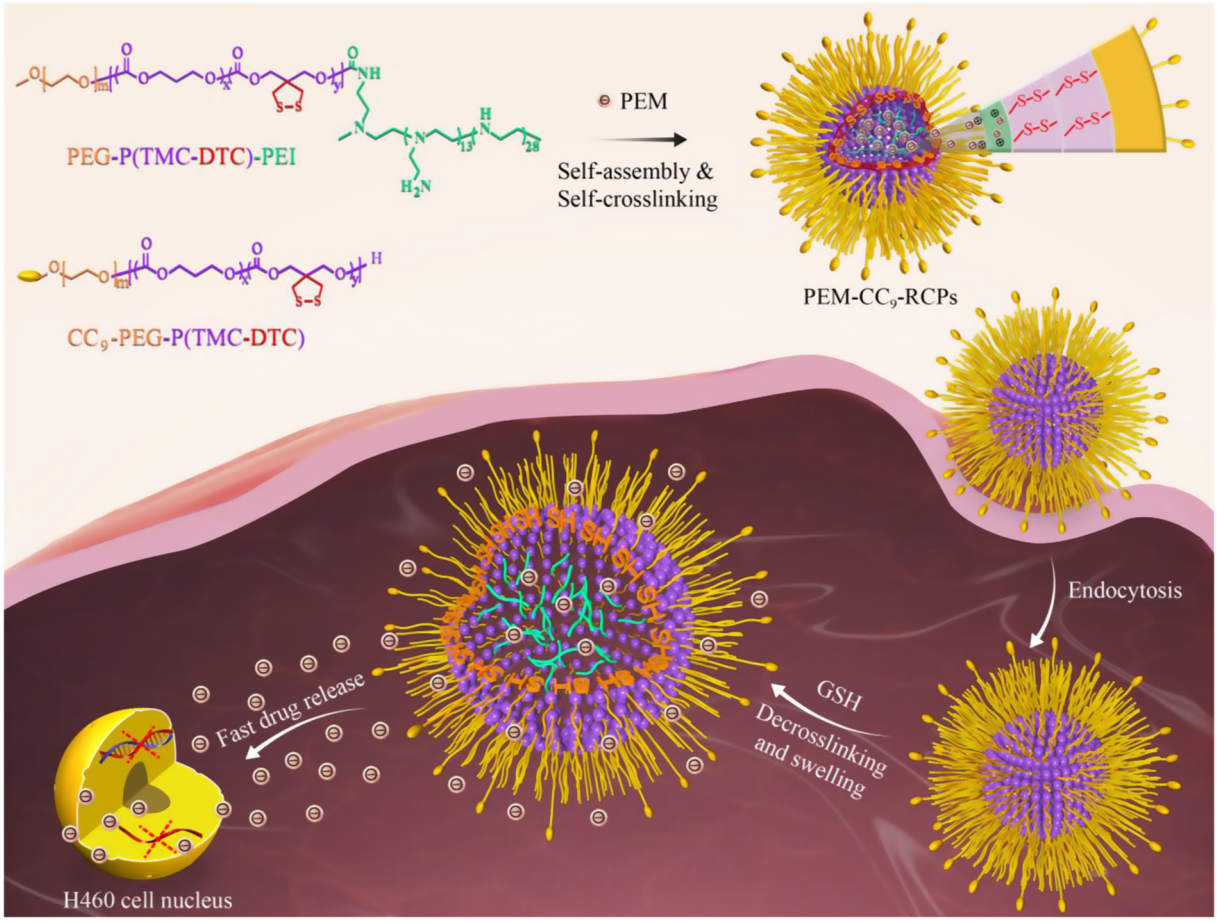

Scheme 1. Schematic illustration of the structure and functions of PEM-CC_9-RCPs in targeted delivery of PEM to H460 cells *in vitro* and *in vivo*.

bearing mice. At 8 and 24 h post injection, the mice were sacrificed. The tumors were collected and sliced (thickness: 4 μm). The blood vessel and cell nuclei were stained with CD31 mAb and DAPI, respectively, for CLSM observation, as described in previous report [24].

2.6. In vivo antitumor performance of PEM-CC_9-RCPs in mice bearing H460 lung tumor

PEM-CC_9-RCPs, PEM-RCPs and Alimta (12.5 mg PEM equiv./kg) were injected via tail veins into H460 tumor bearing mice every 4 days (n = 6). PBS was used as a control. The tumor size and body weight of mice were measured every 2 days and the relative tumor volume and relative body weight were calculated. On day 20, one mouse of each group was sacrificed. The tumors were excised for photographing. The rest five mice were used to determine Kaplan-Meier survival curve within 70 days. Mice in each cohort were considered dead when the mice died during treatment or the tumor volume reached 2000 mm^3.

2.7. Statistical analysis

Data were expressed as mean ± SD. Differences between groups were assessed by one-way ANOVA with Tukey multiple comparison tests. Survival data were analyzed by the Kaplan-Meier technique with a log-rank test for comparison using Graphpad Prism 7. $^{*}p < 0.05$ was considered significant, and $^{**}p < 0.01$, $^{***}p < 0.001$ were considered highly significant.

Results and discussion

3.1. Preparation of CC_9-RCPs and PEM-CC_9-RCPs

CC_9-RCPs were readily prepared by co-self-assembly of two copolymers, PEG-P(TMC-DTC)-PEI with an M_n of 5.0-(14.8–1.8)-1.8 kg/mol and CC_9-functionalized PEG-P(TMC-DTC) with an M_n of 7.5-(15.6–2.3) kg/mol (Fig. S1&S2, Table S1). TNBSA assay of CC_9-PEG-P(TMC-DTC) showed a CC_9 functionality of 93.5%. DLS results demonstrated that CC_9-RCPs with CC_9 densities varying from 0, 4.5%, 9.0% to 13.5% all had small hydrodynamic diameters (51–64 nm, PDI 0.11–0.17) (Fig. 1A, Table S2). The static and dynamic light scattering revealed that CC_9-RCPs with 9.0 mol.% CC_9 had a radius of gyration (R_g) of 28.9 nm and hydrodynamic radius (R_h) of 29 nm, respectively, confirming that they have a vesicular structure (R_g/R_h close to 1) [25]. The vesicular morphology was further corroborated by TEM (Fig. S3A). All CC_9-RCPs had surface charges close to neutral (Table S2), likely due to a chimaeric structure with short PEI mainly orientated in the watery lumen. CC_9-RCPs showed good colloidal stability (Fig. S3A) while fast response to reduction conditions (Fig. S3B), as previously reported for other disulfide-crosslinked nanosystems [23,26].

PEM-CC_9-RCPs were obtained by adding PEM during co-self-assembly process. Notably, PEM-CC_9-RCPs achieved high PEM loading contents of 4.6 to 14.2 wt%, corresponding to loading efficiencies of 92.3% to 66.1%, at theoretical loading contents from 5 to 20 wt% (Table S3), likely due to electrostatic and hydrogen bonding interactions between PEI and PEM. Similar chimaeric polymersomes functionalized with cNGQ peptide have shown a

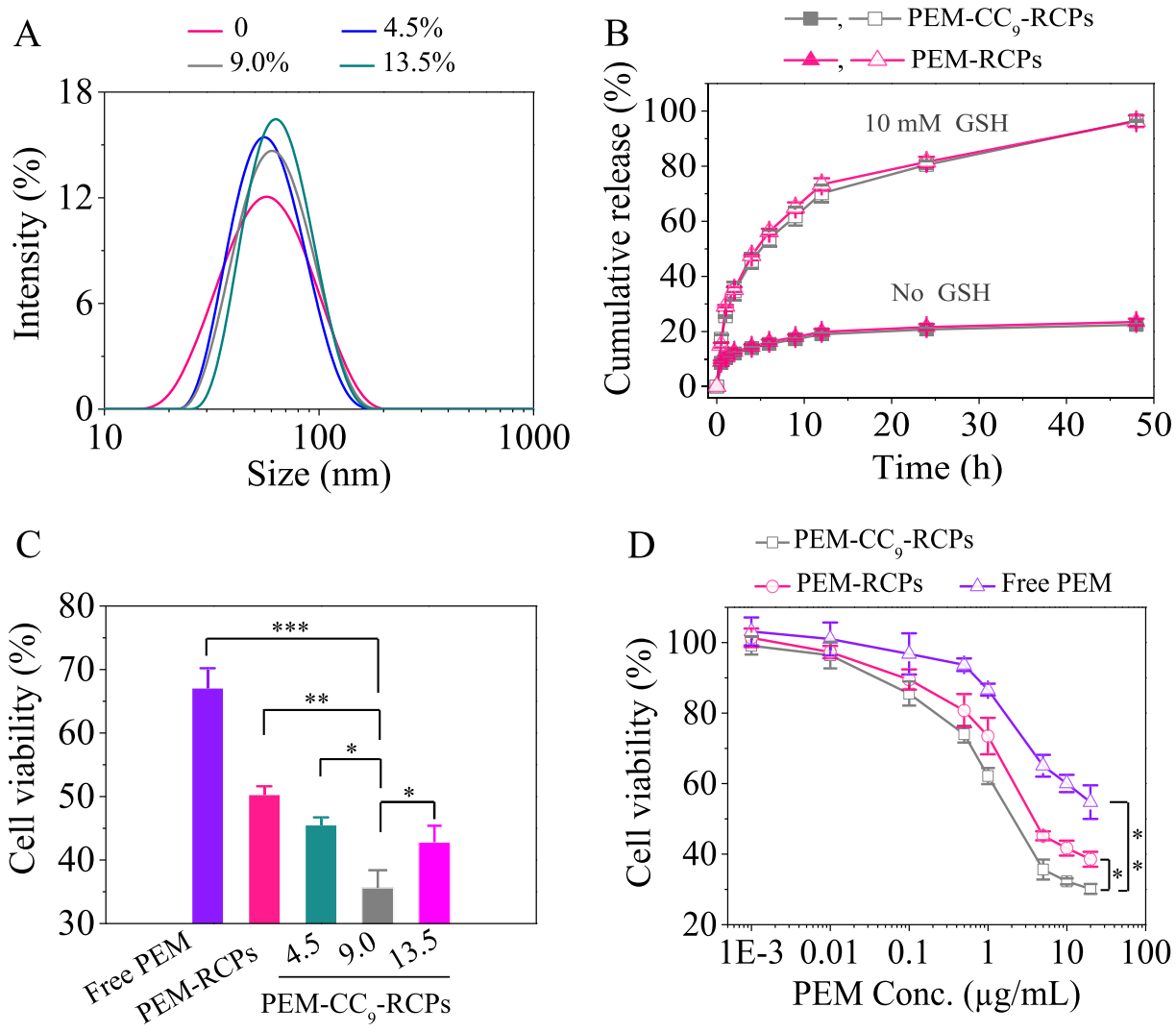

Fig. 1. (A) The influence of CC_9 contents on polymersome hydrodynamic diameter and its distribution. (B) *In vitro* PEM release in PBS in the presence or absence of 10 mM GSH at 37 °C. Polymersome concentration was 50 μg/mL (n = 3). (C) MTT assays of PEM-CC_9-RCPs at 0, 4.5%, 9.0% or 13.5% CC_9 in H460 cells (n = 4). PEM dosage: 5 μg/mL. (D) The concentration-dependent cytotoxicity of PEM-RCPs and PEM-CC_9-RCPs to H460 cells. In C and D, free PEM was used as control. The cells were incubated with different drugs for 4 h and further cultured for 68 h in fresh medium (n = 4). One-way ANOVA with Tukey multiple comparison tests, $^{*}p < 0.05$, $^{**}p < 0.01$, $^{***}p < 0.001$.

high loading of siRNA [19]. PEM-CC_9-RCPs maintained a small hydrodynamic diameter (56–60 nm) and close to neutral zeta potential (Table S3). As expected, only ~23% PEM was released from PEM-CC_9-RCPs in PBS within 48 h whereas quantitative PEM release was observed under 10 mM GSH conditions (Fig. 1B), supporting fast reduction-responsivity. All these results further confirm that CC_9-RCPs possess a chimaeric vesicular structure. MTT assays displayed that PEM-CC_9-RCPs with 9.0 mol.% of CC_9 possessed the best targetability to human H460 lung cancer cells (Fig. 1C). It has been recognized that ligand density plays a significant role in targeting ability of nanomedicines [27–29]. The optimal density depends on particle size, type of ligands and cancer cells. The empty CC_9-RCPs did not cause significant toxicity to H460 cells at tested concentrations up to 0.5 mg/mL (Fig. S3C). It is known that PEI might cause problems for clinical application. However, PEI used in this study has a very low molecular weight of 1.8 kDa, which was reported to have a low cytotoxicity [30–32]. Moreover, as a major feature of this work, PEI is located inside of the polymersome, which will not much influence the biocompatibility of polymersomes. Nevertheless, other low molecular amines like spermine could be considered as a better alternative in the future. In the following, PEM-CC_9-RCPs with 9.0% of CC_9 were used for *in vitro* and *in vivo* experiments if not indicated otherwise. PEM-RCPs (non-targeted control) were prepared with analogous hydrodynamic diameter, drug loading level, surface charge and drug release profiles (Table S3, Fig. 1B).

MTT assays showed a concentration-dependent toxicity of PEM-CC_9-RCPs to H460 cells, with a low IC_{50} of 2.1 μg PEM equiv./mL, which was ca. 2.6 and 10.1-fold lower than that of PEM-RCPs and free PEM, respectively (Fig. 1D), illustrating the active targetability of PEM-CC_9-RCPs to H460 cells. The low cytotoxicity of free PEM was mainly due to its negative charge and inferior cellular uptake. Given the fact that PEM-CC_9-RCPs and PEM-RCPs have a similar drug release profile, the improved anticancer efficacy of PEM-CC_9-RCPs mostly stems from the targeting effect of CC_9.

We then investigated the cellular uptake of Cy5-labeled CC_9-RCPs (CC_9-RCPs-Cy5) in H460 cells. The confocal laser scanning microscope (CLSM) revealed that H460 cells following 8 h incubation with CC_9-RCPs-Cy5 had much stronger Cy5 fluorescence in cytoplasm than RCPs-Cy5 (non-targeted control) (Fig. 2A). The quantitative flow cytometric analyses showed that CC_9-RCPs-Cy5 afforded nearly 2 times stronger Cy5 fluorescence in H460 cells than RCPs-Cy5 (Fig. 2B). This enhancement of uptake by H460 cells was also reported for free CC_9 as compared to PBS control [20]. It

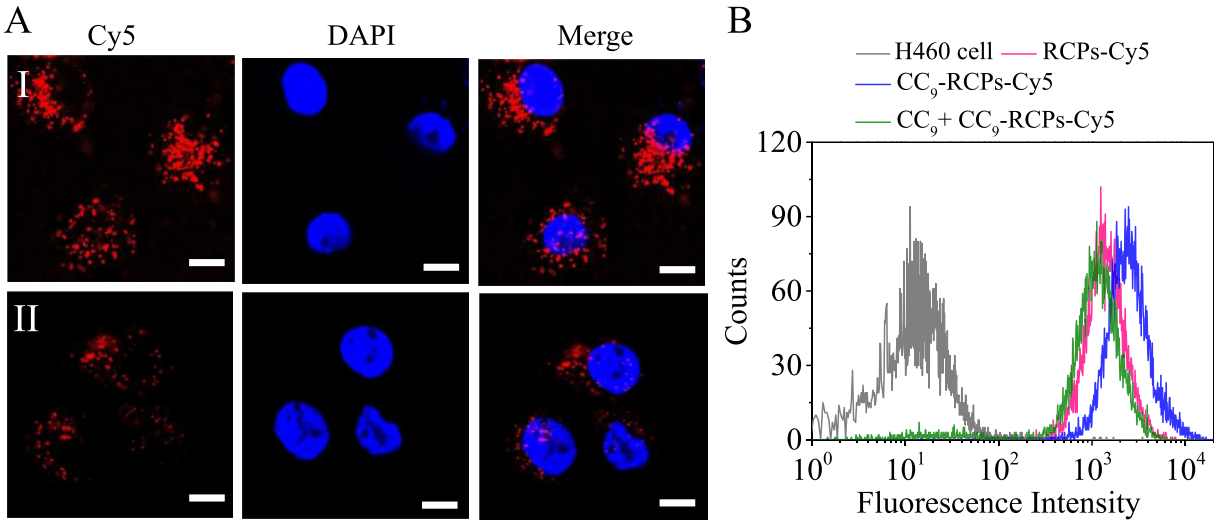

Fig. 2. The cellular uptake of CC_9-RCPs-Cy5 (4 μM Cy5). (A) CLSM images of H460 cells following 8 h incubation with CC_9-RCPs-Cy5 (I) and RCPs-Cy5 (II). Scale bars: 15 μm. (B) Flow cytometric analyses of Cy5 levels in H460 cells incubated with CC_9-RCPs-Cy5 and RCPs-Cy5 for 4 h. PBS was used as control. For competitive studies, H460 cells were pretreated with CC_9 before adding CC_9-RCPs-Cy5. One-way ANOVA with Tukey multiple comparison tests, CC_9-RCPs-Cy5 versus RCPs-Cy5 ($^{*}p < 0.05$), and CC_9-RCPs-Cy5 in H460 cells versus CC_9-RCPs-Cy5 in CC_9 pretreated H460 cells ($^{*}p < 0.05$).

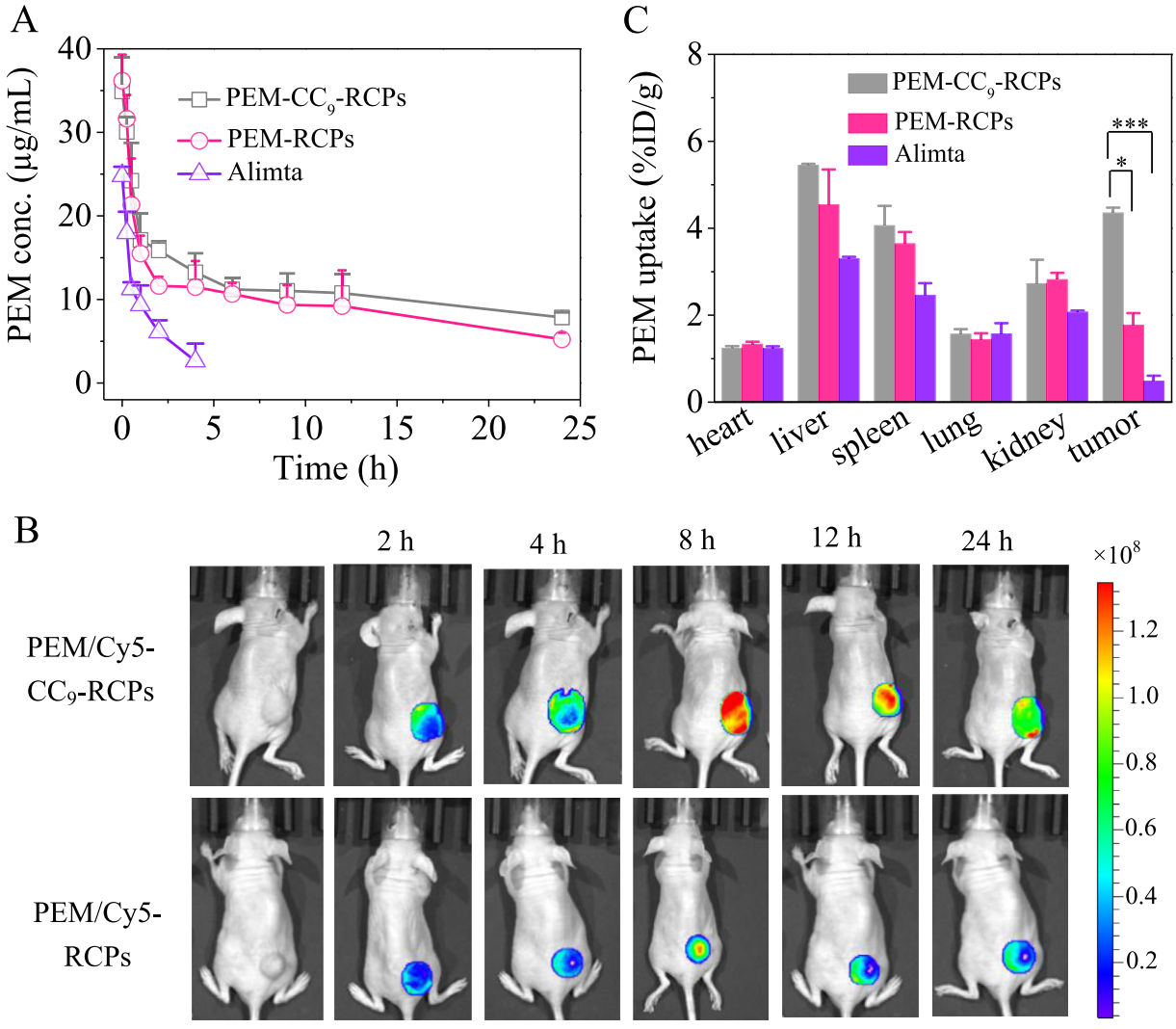

Fig. 3. (A) Blood circulation of PEM-CC_9-RCPs in mice (n = 3). (B) *In vivo* fluorescence imaging of H460 tumor region of nude mice following treating with PEM/Cy5-CC_9-RCPs or non-targeted PEM/Cy5-CC_9-RCPs. (C) *In vivo* biodistribution in H460 tumor-bearing nude mice at 8 h post-injection (n = 3). One-way ANOVA with Tukey multiple comparison tests, $^{*}p < 0.05$, $^{***}p < 0.001$. Dosage: 0.25 mg Cy5 equiv./kg, 12.5 mg PEM equiv./kg.

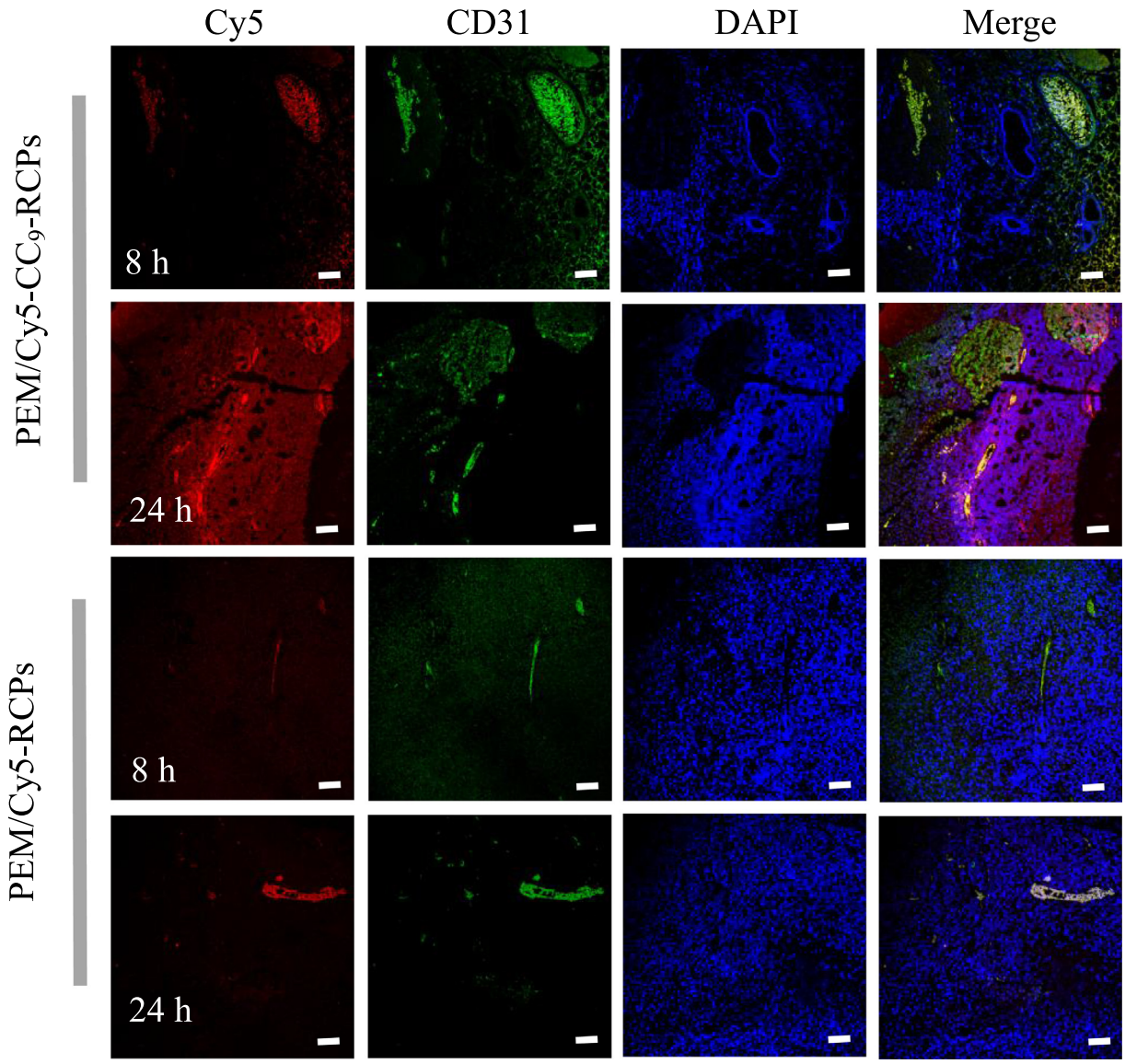

Fig. 4. CLSM images of the central area of tumor slices from H460 tumor-bearing mice treated with PEM/Cy5-CC_9-RCPs or PEM/Cy5-RCPs for 8 or 24 h (0.25 mg Cy5 equiv./kg, 12.5 mg PEM equiv./kg). The distribution of drugs (Cy5), blood vessels (Alexa) and cell nuclei (DAPI) were shown. Scale bar: 100 μm.

should be noted that pretreating H460 cells with free CC_9 resulted in significantly reduced uptake of CC_9-RCPs-Cy5, to a similar level for the non-targeted RCPs-Cy5 control, corroborating that CC_9-RCPs can actively target to H460 lung cancer cells.

3.2. In vivo pharmacokinetics, biodistribution and tumor penetration of PEM-CC_9-RCPs

The pharmacokinetics studies in mice showed that both PEM-CC_9-RCPs and PEM-RCPs had a long elimination half-life ($t_{1/2,\beta}$) of ca. 5.2 h, which was ca. 22-fold longer than clinically used PEM injection Alimta® (Fig. 3A). To monitor their tumor targetability in time, CC_9-RCPs were co-loaded with water-soluble dye Cy5-sulfo and PEM. The *in vivo* fluorescence images showed that mice treated by CC_9-RCPs had obviously stronger Cy5 fluorescence in the tumor than those with non-targeted RCPs counterparts (Fig. 3B). The maximum accumulation occurred at 8 h following injection.

The *in vivo* biodistribution of PEM in the tumors and major organs of H460 tumor-bearing nude mice was quantified using HPLC measurements. Interestingly, PEM-CC_9-RCPs resulted in 4.4%ID/g (injected dose per gram of tissue) in the tumor, which was ca. 2.5 and 9.1-fold higher than PEM-RCPs and Alimta, respectively (Fig. 3C). The tumor-to-normal tissue distribution ratios of PEM-CC_9-RCPs treated H460 tumor bearing mice were 5.4–9.0 and 2.0–2.6 higher than those of Alimta and PEM-RCPs, respectively (Table S4). All the above results point out that PEM-CC_9-RCPs can efficiently target to H460 xenografts in mice.

Tumor penetration is another big concern for nanomedicines [33,34]. We investigated the tumor distribution of Cy5 in H460 tumor-bearing mice after *i.v.* injection of Cy5-coloaded PEM-CC_9-RCPs. CLSM observation of the central area of tumor slices showed that Cy5 fluorescence intensity was weak and mainly located in the blood vessels (stained with CD31) at 8 h post-injection. At 24 h, strong Cy5 fluorescence was observed throughout the whole tumor slices (Fig. 4). Notably, a great deal of Cy5 entered the tumor cells and cell nuclei. As for other nanosystems [35–37], PEM/Cy5-CC_9-RCPs firstly accumulate in the leaky tumor vasculature via so-called "passive targeting". The presence of CC_9 peptide combining with a small particle size of PEM/Cy5-CC_9-RCPs has greatly facilitated tumor penetration by enhancing H460 cell penetration and cytosolic drug release. In contrast, mice treated with Cy5-loaded

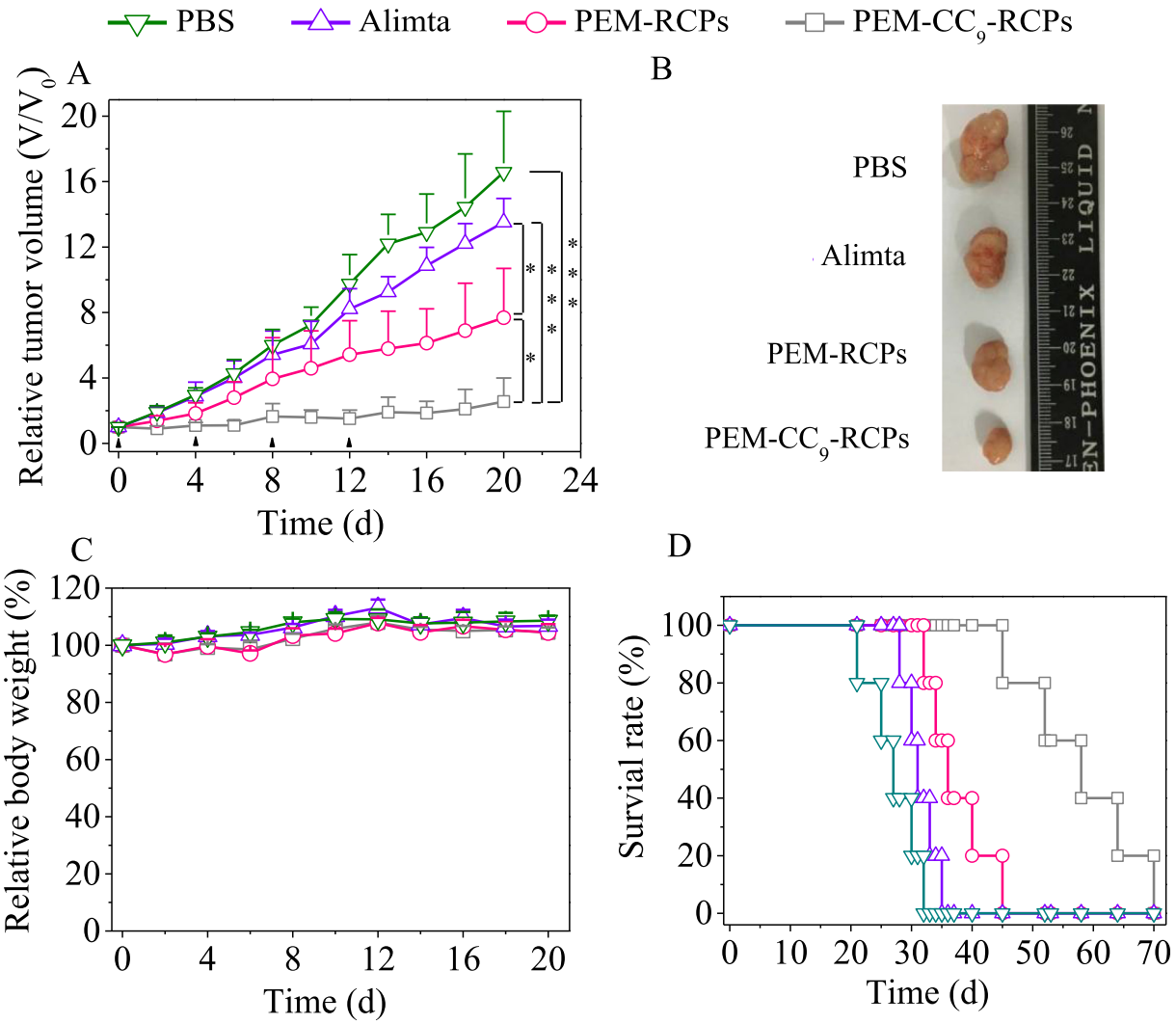

Fig. 5. *In vivo* antitumor performance of PEM-CC_9-RCPs. The drug was given on day 0, 4, 8 and 12 at 12.5 mg PEM equiv./kg. (A) H460 tumor growth inhibition (n = 6). Statistical analysis: One-way ANOVA with Tukey multiple comparison tests, $^{*}p < 0.05$, $^{***}p < 0.001$. (B) The photographs of tumors excised on day 20. (C) Body weight changes of mice (n = 6). (D) Survival curves of mice within 70 d (n = 5). Kaplan-Meier analysis (log-rank test): PEM-CC_9-RCPs vs. PEM-RCPs, Alimta and PBS: $^{**}p < 0.01$; PEM-RCPs vs. Alimta: $^{*}p < 0.05$; PEM-RCPs vs. PBS: $^{**}p < 0.01$.

PEM-RCPs (non-targeted control) had very weak Cy5 fluorescence in the tumor center even at 24 h (Fig. 4). In the past years, different strategies, e.g. by designing tumor microenvironment-sensitive nanoparticles and addition with iRGD peptides [38–46], have been investigated to increase tumor penetration. We recently found that cRGD and TAT dual peptide-functionalized micellar docetaxel penetrated deeply into tumor tissue [47]. The high tumor penetration observed for CC_9-RCPs is likely mainly due to the lung cell selective and penetrating effect of CC_9 peptide [20].

3.3. Antitumor activity of PEM-CC_9-RCPs in H460 tumor bearing nude mice

The therapeutic studies in H460 tumor-bearing nude mice revealed that PEM-CC_9-RCPs induced significantly more effective tumor growth inhibition than Alimta and PEM-RCPs (Fig. 5A). Notably, non-targeted PEM-RCPs showed also better tumor suppression than Alimta. The photographs of tumor burdens excised at 20 d confirmed that PEM-CC_9-RCPs caused the best tumor inhibition (Fig. 5B). No body weight change was observed for all treatment groups (Fig. 5C), confirming good toleration of both PEM-CC_9-RCPs and free PEM. Strikingly, Fig. 5D shows that mice treated with PEM-CC_9-RCPs had greatly improved survival rate than those with PEM-RCPs and Alimta (median survival time: 58 d versus 36 and 31 d, respectively). Hence, reduction-responsive chimaeric polymersomes decorated with lung cancer specific peptide, CSNIDARAC, can efficiently load and transport pemetrexed to H460 human lung tumor xenografts in mice. Ishida *et al.* reported that PEM could not inhibit growth of malignant pleural mesothelioma while PEM in combination with shRNA against thymidylate synthase gene exhibited significantly improved therapeutic efficacy [48]. We have shown previously that cNGQ peptide functionalized RCPs were able to efficiently load and deliver siRNA to lung tumor [19]. CC_9-RCPs might provide also a unique platform for combination cancer therapy (e.g. chemotherapy with PEM and gene therapy with siRNA or shRNA). Furthermore, the blood analyses of Balb/c mice at 24 h post-injection of 12.5 mg PEM equiv./kg PEM-CC9-RCPs showed comparable levels of ALT, AST, serum creatinine and blood urea nitrogen to those with PBS control (Fig. S4), indicating the absence of hepatic and kidney toxicity. Therefore, PEM-CC_9-RCPs have an excellent safety profile, which makes them interesting for possible clinical translation.

Conclusion

We have shown that PEM-loaded, CC_9-directed and reversibly-crosslinked chimaeric polymersomes (PEM-CC_9-RCPs) have many appealing properties such as small hydrodynamic diameter (60 nm), high PEM loading (up to 14.2 wt%), excellent stability, fast reduction-responsivity and high H460 tumor cell specificity. The *in vivo* results reveal that PEM-CC_9-RCPs while maintaining a long circulation time display markedly improved tumor accumulation and superior tumor penetration as compared to the non-targeted PEM-RCPs control in H460 tumor-bearing nude mice. The therapeutic studies demonstrate that PEM-CC_9-RCPs bring about significantly more effective tumor growth suppression and better survival rate in H460 tumor-bearing mice than clinically used PEM injection Alimta, without causing obvious systemic toxicity. To the best of our knowledge, this represents a first report on targeted nanosystems that are capable of efficient loading and targeted delivery of pemetrexed to lung tumors. Considering their excellent safety profile, facile synthesis and ease of scaling up production, these pemetrexed-loaded, lung cancer specific and reduction-responsive chimaeric polymersomes have a great potential for translating into treatment of lung tumors in humans.

Acknowledgements

This work is financially supported by research grants from the National Natural Science Foundation of China (51473111, 51773146, 51561135010, 51633005).

Appendix A. Supplementary data

Supplementary data associated with this article can be found, in the online version, at https://doi.org/10.1016/j.actbio.2018.01.015.

References

[1] R.L. Siegel, K.D. Miller, A. Jemal, Cancer statistics, CA-Cancer J. Clin. 66 (2016) (2016) 7–30.
[2] T.J. Lynch, D.W. Bell, R. Sordella, S. Gurubhagavatula, R.A. Okimoto, B.W. Brannigan, P.L. Harris, S.M. Haserlat, J.G. Supko, F.G. Haluska, Activating mutations in the epidermal growth factor receptor underlying responsiveness of non-small-cell lung cancer to gefitinib, New Engl. J. Med. 350 (2004) 2129–2139.
[3] R. Rosell, E. Carcereny, R. Gervais, A. Vergnenegre, B. Massuti, E. Felip, R. Palmero, R. Garcia-Gomez, C. Pallares, J.M. Sanchez, Erlotinib versus standard chemotherapy as first-line treatment for European patients with advanced EGFR mutation-positive non-small-cell lung cancer (EURTAC): a multicentre, open-label, randomised phase 3 trial, Lancet Oncol. 13 (2012) 239–246.
[4] J.M. Sun, J.S. Ahn, S.H. Jung, J. Sun, S.Y. Ha, J. Han, K. Park, M.J. Ahn, Pemetrexed plus cisplatin versus gemcitabine plus cisplatin according to thymidylate synthase expression in nonsquamous non-small-cell lung cancer: a biomarker-stratified randomized phase II trial, J. Clin. Oncol. 33 (2015) 2450–2456.
[5] P.M. Fidias, S.R. Dakhil, A.P. Lyss, D.M. Loesch, D.M. Waterhouse, J.L. Bromund, R. Chen, M. Hristova-Kazmierski, J. Treat, C.K. Obasaju, Phase III study of immediate compared with delayed docetaxel after front-line therapy with gemcitabine plus carboplatin in advanced non-small-cell lung cancer, J. Clin. Oncol. 27 (2008) 591–598.
[6] M.A. Socinski, I. Bondarenko, N.A. Karaseva, A.M. Makhson, I. Vynnychenko, I. Okamoto, J.K. Hon, V. Hirsh, P. Bhar, H. Zhang, Weekly nab-paclitaxel in combination with carboplatin versus solvent-based paclitaxel plus carboplatin as first-line therapy in patients with advanced non-small-cell lung cancer: final results of a phase III trial, J. Clin. Oncol. 30 (2012) 2055–2062.
[7] M. Vandana, S.K. Sahoo, Reduced folate carrier independent internalization of PEGylated pemetrexed: a potential nanomedicinal approach for breast cancer therapy, Mol. Pharm. 9 (2012) 2828–2843.
[8] S. Senan, A. Brade, L.H. Wang, J. Vansteenkiste, S. Dakhil, B. Biesma, A.M. Martinez, J. Aerts, R. Govindan, B. Rubio-Viqueira, Proclaim: Randomized phase III trial of pemetrexed-cisplatin or etoposide-cisplatin plus thoracic radiation therapy followed by consolidation chemotherapy in locally advanced nonsquamous non-small-cell lung cancer, J. Clin. Oncol. 34 (2016) 953–962.
[9] J.D. Patel, T.A. Hensing, A. Rademaker, E.M. Hart, M.G. Blum, D.T. Milton, P.D. Bonomi, Phase II study of pemetrexed and carboplatin plus bevacizumab with maintenance pemetrexed and bevacizumab as first-line therapy for nonsquamous non-small-cell lung cancer, J. Clin. Oncol. 27 (2009) 3284–3289.
[10] E. Smit, K. Mattson, J. Von Pawel, C. Manegold, S. Clarke, P. Postmus, ALIMTA®(pemetrexed disodium) as second-line treatment of non-small-cell lung cancer: a phase II study, Ann. Oncol. 14 (2003) 455–460.
[11] N. Katirtzoglou, I. Gkiozos, N. Makrilia, E. Tsaroucha, A. Rapti, G. Stratakos, G. Fountzilas, K.N. Syrigos, Carboplatin plus pemetrexed as first-line treatment of patients with malignant pleural mesothelioma: a phase II study, Clin. Lung Cancer 11 (2010) 30–35.
[12] K.M. Li, L.P. Rivory, S.J. Clarke, Pemetrexed pharmacokinetics and pharmacodynamics in a phase I/II study of doublet chemotherapy with vinorelbine: implications for further optimisation of pemetrexed schedules, Brit. J. Cancer 97 (2007) 1071–1076.
[13] I.G. Glezerman, M.C. Pietanza, V. Miller, S.V. Seshan, Kidney tubular toxicity of maintenance pemetrexed therapy, Am. J. Kidney Dis. 58 (2011) 817–820.
[14] X. Zhang, Y. Zheng, Z. Wang, S. Huang, Y. Chen, W. Jiang, H. Zhang, M. Ding, Q. Li, X. Xiao, Methotrexate-loaded PLGA nanobubbles for ultrasound imaging and Synergistic Targeted therapy of residual tumor during HIFU ablation, Biomaterials 35 (2014) 5148–5161.
[15] S. Jain, R. Mathur, M. Das, N.K. Swarnakar, A.K. Mishra, Synthesis, pharmacoscintigraphic evaluation and antitumor efficacy of methotrexate-loaded, folate-conjugated, stealth albumin nanoparticles, Nanomedicine 6 (2011) 1733–1754.
[16] N.N. Lu, R.T. Li, Q. Liu, B. Hu, X.L. Xu, C.S. Ji, X.H. Han, P. Wang, B.R. Liu, Antitumor and antimetastatic effects of pemetrexed-loaded targeted nanoparticles in B16 bearing mice, Drug Deliv. 23 (2015) 1–9.
[17] N.E. Eldin, A.S. Abu Lila, K. Kawazoe, H.M. Elnahas, M.A. Mahdy, T. Ishida. Encapsulation in a rapid-release liposomal formulation enhances the anti-tumor efficacy of pemetrexed in a murine solid mesothelioma-xenograft model, Eur. J. Pharm. Sci. 81 (2016) 60–66.
[18] W.J. Yang, Y. Zou, F.H. Meng, J. Zhang, R. Cheng, C. Deng, Z.Y. Zhong, Efficient and targeted suppression of human lung tumor xenografts in mice with methotrexate sodium encapsulated in all-function-in-one chimeric polymersomes, Adv. Mater. 28 (2016) 8234–8239.
[19] Y. Zou, M. Zheng, W.J. Yang, F.H. Meng, K. Miyata, H.J. Kim, K. Kataoka, Z.Y. Zhong, Virus-mimicking chimaeric polymersome boosts targeted cancer siRNA therapy *in vivo*, Adv. Mater. 29 (2017), https://doi.org/10.1002/adma.201703285.
[20] X. He, M.H. Na, J.S. Kim, G.Y. Lee, J.Y. Park, A.S. Hoffman, J.O. Nam, S.E. Han, G.Y. Sim, Y.K. Oh, I.S. Kim, B.H. Lee, A novel peptide probe for imaging and targeted delivery of liposomal doxorubicin to lung tumor, Mol. Pharm. 8 (2011) 430–438.
[21] Y. Fang, W.J. Yang, L. Cheng, F.H. Meng, J. Zhang, Z.Y. Zhong, EGFR-targeted multifunctional polymersomal doxorubicin induces selective and potent suppression of orthotopic human liver cancer in vivo, Acta Biomater. 64 (2017) 323–333.
[22] Y. Fang, Y. Jiang, Y. Zou, F.H. Meng, J. Zhang, C. Deng, H.L. Sun, Z.Y. Zhong, Targeted glioma chemotherapy by cyclic RGD peptide-functionalized reversibly core-crosslinked multifunctional poly (ethylene glycol)-*b*-poly (ε-caprolactone) micelles, Acta Biomater. 50 (2017) 396–406.
[23] N. Zhang, Y.F. Xia, Y. Zou, W.J. Yang, J. Zhang, Z.Y. Zhong, F.H. Meng, ATN-161 peptide functionalized reversibly cross-linked polymersomes mediate targeted doxorubicin delivery into melanoma-bearing C57BL/6 mice, Mol. Pharm. 14 (2017) 2538–2547.
[24] Y.Q. Zhu, X.X. Wang, J. Chen, J. Zhang, F.H. Meng, C. Deng, R. Cheng, J. Feijen, Z. Y. Zhong, Bioresponsive and fluorescent hyaluronic acid-iodixanol nanogels for targeted X-ray computed tomography imaging and chemotherapy of breast tumors, J. Control. Release 244 (2016) 229–239.
[25] T. Nie, Y. Zhao, Z.W. Xie, C. Wu, Micellar formation of poly (caprolactone-block-ethylene oxide-lock-caprolactone) and its enzymatic biodegradation in aqueous dispersion, Macromolecules 36 (2003) 8825–8829.
[26] Y. Zou, F.H. Meng, C. Deng, Z.Y. Zhong, Robust, tumor-homing and redox-sensitive polymersomal doxorubicin: a superior alternative to Doxil and Caelyx?, J Control. Release 239 (2016) 149–158.
[27] D.R. Elias, A. Poloukhtine, V. Popik, A. Tsourkas, Effect of ligand density, receptor density, and nanoparticle size on cell targeting, Nanomed-Nanotechnol. 9 (2013) 194–201.
[28] Y.N. Zhong, F.H. Meng, C. Deng, Z.Y. Zhong, Ligand-directed active tumor-targeting polymeric nanoparticles for cancer chemotherapy, Biomacromolecules 15 (2014) 1955–1969.
[29] N. Kamaly, Z. Xiao, P.M. Valencia, A.F. Radovic-Moreno, O.C. Farokhzad, Targeted polymeric therapeutic nanoparticles: design, development and clinical translation, Chem. Soc. Rev. 41 (2012) 2971–3010.
[30] W. Wang, M. Balk, Z. Deng, C. Wischke, M. Gossen, M. Behl, N. Ma, A. Lendlein, Engineering biodegradable micelles of polyethylenimine-based amphiphilic block copolymers for efficient DNA and siRNA delivery, J. Control. Release 242 (2016) 71–79.
[31] A. Ewe, A. Schaper, S. Barnert, R. Schubert, A. Temme, U. Bakowsky, A. Aigner, Storage stability of optimal liposome-polyethylenimine complexes (lipopolyplexes) for DNA or siRNA delivery, Acta Biomater. 10 (2014) 2663–2673.
[32] K. Kunath, H.A. Von, D. Fischer, H. Petersen, U. Bickel, K. Voigt, T. Kissel, Low-molecular-weight polyethylenimine as a non-viral vector for DNA delivery: comparison of physicochemical properties, transfection efficiency and in vivo distribution with high-molecular-weight polyethylenimine, J. Control. Release 89 (2003) 113–125.
[33] E. Ruoslahti, Peptides as targeting elements and tissue penetration devices for nanoparticles, Adv. Mater. 24 (2012) 3747–3756.

[34] R.K. Jain, T. Stylianopoulos, Delivering nanomedicine to solid tumors, Nat. Rev. Clin. Oncol. 7 (2010) 653–664.
[35] H. Maeda, Toward a full understanding of the EPR effect in primary and metastatic tumors as well as issues related to its heterogeneity Adv, Drug Deliver. Rev. 91 (2015) 3–6.
[36] D. Peer, J.M. Karp, S. Hong, O.C. Farokhzad, R. Margalit, R. Langer, Nanocarriers as an emerging platform for cancer therapy, Nat. Nanotechnol. 2 (2007) 751–760.
[37] H. Maeda, H. Nakamura, J. Fang, The EPR effect for macromolecular drug delivery to solid tumors: improvement of tumor uptake, lowering of systemic toxicity, and distinct tumor imaging in vivo, Adv. Drug Deliver. Rev. 65 (2013) 71–79.
[38] J.H. Su, H.P. Sun, Q.S. Meng, Q. Yin, S. Tang, P.C. Zhang, Y. Chen, Z.W. Zhang, H.J. Yu, Y.P. Li, Long circulation red-blood-cell-mimetic nanoparticles with peptide-enhanced tumor penetration for simultaneously inhibiting growth and lung metastasis of breast cancer, Adv. Funct. Mater. 26 (2016) 1243–1252.
[39] Z. Hao, Z. Fan, J. Deng, P.K. Lemons, D.C. Arhontoulis, W.B. Bowne, C. Hao, Hyaluronidase embedded in nanocarrier PEG shell for enhanced tumor penetration and highly efficient antitumor efficacy, Nano Lett. 16 (2016) 3268–3277.
[40] T. Ji, Y. Ding, Y. Zhao, J. Wang, H. Qin, X. Liu, J. Lang, R. Zhao, Y. Zhang, J. Shi, N. Tao, Z. Qin, G. Nie, Peptide assembly integration of fibroblast-targeting and cell-penetration features for enhanced antitumor drug delivery, Adv. Mater. 27 (2015) 1865–1873.
[41] H.J. Li, J.Z. Du, X.J. Du, C.F. Xu, C.Y. Sun, H.X. Wang, Z.T. Cao, X.Z. Yang, Y.H. Zhu, S.M. Nie, J. Wang, Stimuli-responsive clustered nanoparticles for improved tumor penetration and therapeutic efficacy, Proc. Natl. Acad. Sci. U.S.A. 113 (2016) 4164–4169.
[42] Q. Lei, S.B. Wang, J.J. Hu, Y.X. Lin, C.H. Zhu, L. Rong, X.Z. Zhang, Stimuli-responsive "cluster bomb" for programmed tumor therapy, ACS Nano 11 (2017) 7201–7214.
[43] L.H. Liu, W.X. Qiu, Y.H. Zhang, B. Li, C. Zhang, F. Gao, L. Zhang, X.Z. Zhang, A charge reversible self-delivery chimeric peptide with cell membrane-targeting properties for enhanced photodynamic therapy, Adv. Funct. Mater. (2017), https://doi.org/10.1002/adfm.201700220.
[44] J.J. Chen, J.X. Ding, Y.C. Wang, J.J. Cheng, S.X. Ji, X.L. Zhuang, X.S. Chen, Sequentially responsive shell-stacked nanoparticles for deep penetration into solid tumors, Adv. Mater. 29 (2017), https://doi.org/10.1002/adma.201701170.
[45] Q. Hu, W. Sun, Y. Lu, H.N. Bomba, Y. Ye, T. Jiang, A.J. Isaacson, Z. Gu, Tumor microenvironment-mediated construction and deconstruction of extracellular drug-delivery depots, Nano Lett. 16 (2016) 1118–1126.
[46] S. Ruan, X. Cao, X. Cun, G. Hu, Y. Zhou, Y. Zhang, L. Lu, Q. He, H. Gao, Matrix metalloproteinase-sensitive size-shrinkable nanoparticles for deep tumor penetration and pH triggered doxorubicin release, Biomaterials 60 (2015) 100–110.
[47] Y.Q. Zhu, J. Zhang, F.H. Meng, C. Deng, R. Cheng, J. Feijen, Z.Y. Zhong, cRGD/TAT dual-ligand reversibly crosslinked micelles loaded with docetaxel penetrate deeply into tumor tissue and show high antitumor efficacy in vivo, ACS Appl. Mater. Inter. 9 (2017) 35651–35663.
[48] A.S.A. Lila, M. Fukushima, C.L. Huang, H. Wada, T. Ishida, Systemically administered RNAi molecule sensitizes malignant pleural mesothelioma cells to pemetrexed therapy, Mol. Pharm. 13 (2016) 3955–3963.